Remote Sens. **2015**, *7*, 5951-5979; doi:10.3390/rs70505951

OPEN ACCESS

remote sensing

ISSN 2072-4292

www.mdpi.com/journal/remotesensing

Article

Impact of Sowing Date on Yield and Water Use Efficiency of Wheat Analyzed through Spatial Modeling and FORMOSAT-2 Images

Benoit Duchemin [1], Rémy Fieuzal [1,*], Miguel Augustin Rivera [2], Jamal Ezzahar [3], Lionel Jarlan [1], Julio César Rodriguez [4], Olivier Hagolle [1] and Christopher Watts [4]

[1] CESBIO—UMR CNRS-CNES-IRD-UPS, 18 Av. EdouardBelin, BPI 280, Toulouse Cedex 9, France; E-Mails: benoit.duchemin@cesbio.cnes.fr (B.D.); lionel.jarlan@cesbio.cnes.fr (L.J.); olivier.hagolle@cesbio.cnes.fr (O.H.)

[2] ITSON, Departamento de Cienciasdel Agua y del Medio Ambiente, 5 de Febrero 818 Sur, Cd. Obregón, Sonora 85000, Mexico; E-Mail: mrivera@itson.mx

[3] Faculté des Sciences Semlalia, Boulevard Prince My Abdellah, B.P. 2390, 40000 Marrakech, Maroc; E-Mail: j.ezzahar@gmail.com

[4] UNISON, Blvd. Luis Encinas y Rosales S/N, Col. Centro, Hermosillo, Sonora 83000, Mexico; E-Mails: jcrod@raramuri.fisica.uson.mx (J.C.R.); watts@raramuri.fisica.uson.mx (C.W.)

* Author to whom correspondence should be addressed; E-Mail: remy.fieuzal@cesbio.cnes.fr; Tel.: +33-5-6261-7340.

Academic Editors: Yoshio Inoue and Prasad S. Thenkabail

Received: 1 July 2014 / Accepted: 20 April 2015 / Published: 13 May 2015

Abstract: Regional analysis of water use efficiency (WUE) is a relevant method for diagnosing the performance of irrigation systems in water-limited environments. In this study, we investigated the potential of FORMOSAT-2 images to provide spatial estimates of WUE over irrigated wheat crops cultivated within the semi-arid Yaqui Valley, in the northwest of Mexico. FORMOSAT-2 provided us with a unique dataset of 36 images at a high resolution (8 m) encompassing the wheat growing season from November 2007 to May 2008. Time series of green leaf area index were derived from these satellite images and used to calibrate a simple crop/water balance model. The method was applied over an 8 × 8 km^2 irrigated area on up to 530 wheat fields. It allowed us to accurately reproduce the time courses of Leaf Area Index and dry aboveground biomass, as well as evapotranspiration and soil moisture. In a second step, we analyzed the variations of WUE as the ratio of accumulated dry aboveground biomass to seasonal evapotranspiration. Despite the study

area being rather small and homogeneous (soil, climate), we observed a large range in wheat biomass production, from 5 to 15 $t \cdot ha^{-1}$, which was primarily related to the timing of plant emergence. In contrast, the seasonal evapotranspiration only varied from 350 to 450 mm, with no evident link with sowing practices. A significant gain in crop water productivity was found for the fields sown the earliest (maximal WUE around 3.5 $kg \cdot m^{-3}$) compared to those sown the latest (minimal WUE around 1.5 $kg \cdot m^{-3}$). These results demonstrated the value of the FORMOSAT-2 images to provide spatial estimates of crop production and water consumption. The detailed information provided by such high space and time resolution imaging systems is highly valuable to identify agricultural practices that could enlarge crop water productivity.

Keywords: remote sensing; FORMOSAT; crop model; water balance; evapotranspiration; biomass production; wheat; water use efficiency; sowing; irrigation

1. Introduction

Agriculture is facing many challenges, amongst which are the maintenance of a highly-productive system and the protection of water resources. Although irrigated agriculture covers less than 20 percent of total cropland, it contributes to 40 percent of global food production [1,2]. Agriculture is by far the largest consumer of water with about 70% of the renewable resource used for irrigation [3]. Water-scarce countries are often not able to meet their food requirements using the water resource available within their boundaries [4,5], and the number of countries and regions without enough water to produce their food is continually rising as the population increases and as climatic variability is greater than ever. Low latitude semi-arid areas are specifically in jeopardy, with a likelihood of reduced precipitation, more variable rainfall distribution and more frequent extreme events as a consequence of climatic change [6]. There is thus a continuous demand for improving agricultural water management, especially in semi-arid areas, such as the Mediterranean countries, for which [7] have recognized three types of strategies: (i) organizing irrigation supply through an accurate calculation of crop water needs; (ii) improving the performance of irrigation techniques and networks; and (iii) selecting species and plant varieties that enhance water use. This demand primarily concerns cereals: 50% of the world's cereal production comes from irrigated croplands, amongst which up to 80% is in developing countries [8]; maize, rice and wheat provide about 60% of human calories, either directly or indirectly as food for livestock [9].

With about 550,000 billion tons produced yearly on about 25% of all agricultural lands (FAO statistics), wheat is the most important cereal. The semi-arid Yaqui Valley is the most productive area in Mexico, which contributes roughly 40% of the national wheat production [10]. In this region, irrigated wheat crops cover about 140,000 ha between the Sierra Madre and the Gulf of California. The Yaqui Valley was the home place of the Green Revolution, where wheat yield has known an impressive rise from about 2.0 $t \cdot ha^{-1}$ in 1960 to 5.0 $t \cdot ha^{-1}$ in 1980 [11]. However, yield stagnation has been observed during the post Green Revolution period since 1980 [9], and extreme weather events that affected the world during the 1990s have also been very marked in the region. Indeed, a severe

drought was observed from 1994 to 2002 in northern Mexico [12,13], which resulted in an emptying of the reservoirs. The 19 dams located on the rivers of the Gulf of California contained less than 20% of their storage capacity in 1999 [12], and by May 2000, the main reservoir levels had slipped under "dead storage", *i.e.*, the point at which the remaining water was accessible only by pumping [11,14,15]. This climatic crisis resulted in an increase of groundwater use and in a reduction of the crop production: sown areas have recovered less than 25% of the whole Yaqui Valley during the 2003 to 2004 agricultural season [14,16]. This historical overview highlights that diagnosing and improvement studies for an efficient use of agricultural water should continue in this region.

Agricultural production and water resources were associated with the concept of water use efficiency (WUE) since the beginning of the 19th century [17]. Though many definitions co-exist in agricultural sciences [18–20], WUE is commonly defined as the ratio of yield-to-water consumption, the water consumption being approximated by evapotranspiration and the yield referring to either the global dry matter or the marketable crop yield [7]. WUE is an important indicator for agricultural water management in water-limited environments [21]. It is meaningful to analyze the plant-water relationship in order to compare the performance between various irrigation methods, agricultural practices (e.g., sowing date, fertilizer, row spacing), species, varieties and agro-climatic conditions [7,22–25]. Amongst the different strategies that increase WUE, synchronizing crop calendars with periods during which crop water needs are minimal and/or can be fulfilled by rainfall is often the first and foremost step [26]. Analyzing WUE at the level of irrigation projects remains useful, though care should be taken, since many agro-environmental inputs affect crop growth [27].

A regional analysis of water use efficiency requires spatial data for integrating land cover features, as well as hydrological and vegetation parameters. Remote sensing may be the only feasible means of providing such information on a consistent space and time basis. Until now, optical images have been acquired from space either by high-resolution sensors (e.g., Landsat-TM or SPOT-HRV), which provide data at 10-m to 30-m resolution with moderate revisit capacities (around 15 days), or by large field-of-view systems (e.g., SPOT-VEGETATION, TERRA-MODIS) that observe the Earth on a daily basis, but under a large range of viewing angles and at a much coarser spatial resolution (250 m to 1 km). Launched in 2004, the FORMOSAT-2 Taiwanese satellite has the unique capacity to acquire daily images at 8-m spatial resolution with a constant viewing angle [28]. It is particularly convenient to monitor agricultural areas, which are often made of a juxtaposition of small, more or less homogeneous units (fields) with a high temporal dynamics due to the vegetation phenological cycle (growth and senescence in a few months for annual crops) and agricultural operations (sowing, plowing, irrigation, harvest *etc*.). The high density of mono-directional FORMOSAT-2 observations has allowed improving image preprocessing (cloud detection and atmospheric correction) and obtaining very accurate time series of surface reflectances and vegetation indices [29]. A few studies have demonstrated the usefulness of time series of FORMOSAT-2 images for the mapping of land cover, the detection of agricultural operations and the monitoring of several key biophysical variables [30–34].

In this context, the objective of this study is two-fold: (i) to demonstrate the value of FORMOSAT-2 images combined with a simple crop/water balance model for spatial estimates of seasonal evapotranspiration, biomass production and crop water productivity; and (ii) to study the relationship between these variables and sowing dates in order to identify sowing practices that have increased water use efficiency for wheat crops cultivated in the Yaqui Valley during the 2007 to 2008 season.

2. Materiel and Methods

2.1. Study Area

The experiment took place during the 2007 to 2008 agricultural season within the Yaqui Valley, a very large and flat agricultural area in the northwest of Mexico. The climate of this region is hot and semi-arid: mean daily temperature ranges from 17 °C in January to 31 °C in July and August; annual rainfall is on average about 320 mm, amongst which 70% falls during summer. Irrigation water is transported by 2 large channels that may transfer up to 100 $m^3 \cdot s^{-1}$. It comes from the precipitation over the Sierra Madre, which is stored in several dams built over the Yaqui River system. The extent of the total irrigated surface in the valley exceeds 225,000 ha, 60% of which is covered by winter wheat cultivated from November to May. The region produces some of the highest wheat yield in the world, resulting from a combination of irrigation, high fertilizer rates and modern cultivars. The Yaqui Valley was documented for many years as the "home of the Green Revolution for wheat" in developing countries; an abundant literature dealing with various climatic, environmental, hydrological and political issues related to agricultural water management is available, amongst which are the articles previously cited in the Introduction, as well as [35–45].

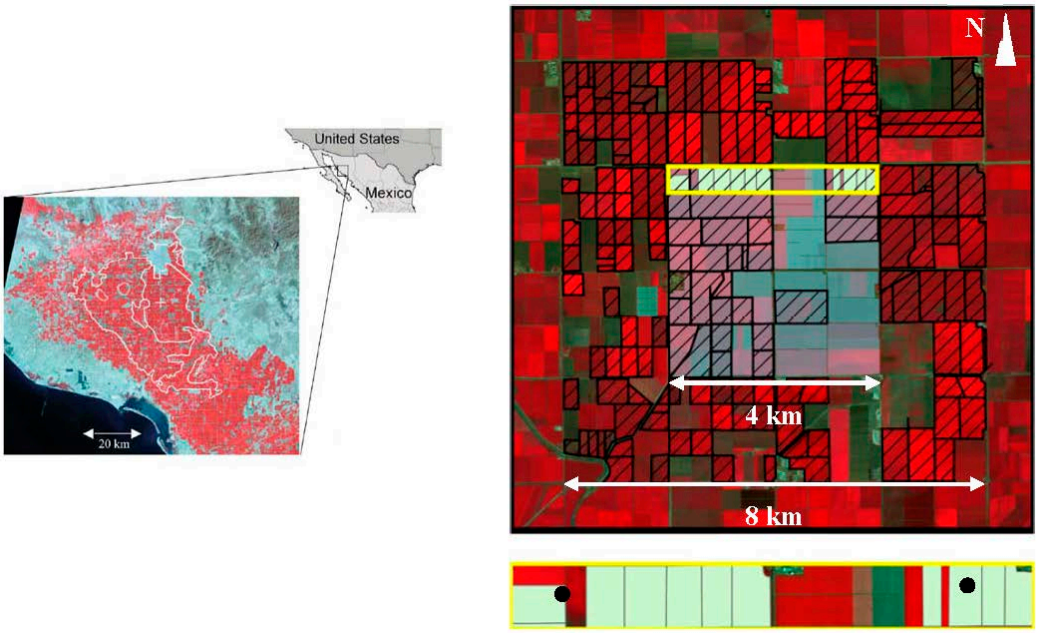

Figure 1. Location of the Yaqui Valley in the northwest of Mexico (**left**). The 8 × 8 km^2 study area is delineated on a FORMOSAT-2 image, with its 4 × 4 km^2 central part highlighted (**right**). Wheat fields are hatched in black. The bottom zoomed yellow area shows fields where grain yields were collected (in green). The two black discs highlight the location of the micro-meteorological stations installed on the wheat fields.

During the experiment, we focused on an 8 × 8 km^2 study area located 40 km south of Ciudad Obregon (27.25°N, 109.88°W), which is organized in large fields along irrigation channels every 2 km (Figure 1). According to soil map (Plano unico, Distrito de Riego del Rio Yaqui (S. de R.L. de I.P. Y C.V. (Sociedad de Responsabilidad Limitada de Interés Público Y Capital Variable), Gerencia

General del Distrito), scale 1:200,000), the soil is rather homogeneous, of clay-sandy type, with a depth larger than 1 m and poor in organic matter (<1%). It is representative of Vertisols located within the Yaqui Valley outer coast and riverbeds [42]. The land use was exhaustively recorded over the 8 × 8 km^2 study area, which was covered by about 60% wheat crops during the 2007 to 2008 agricultural season (Figure 1). Agricultural practices and biophysical data were collected by scientific equipment and field enquiry for all wheat fields within the 4 × 4 km^2 square located at the center of the study area. This square is referred to as the central zone hereinafter.

2.2. Experimental Data

Wheat fields within the 4 × 4 km^2 central zone were intensively monitored over the 2007 to 2008 agricultural season in order to acquire the following data: climatic data, micro-meteorological data, agricultural practices, vegetation- and soil-biophysical variables.

Climatic data were collected by standard meteorological stations installed within and around the central zone between September 2007 and June 2008. Solar radiation, air temperature, wind speed, air relative humidity, atmospheric pressure and precipitation were acquired at a 2-m height every 30 min. Half-hourly measurements were averaged or accumulated to obtain daily values of air temperature, global incoming radiation and precipitation.

Micro-meteorological data were collected on two wheat fields located at the northwest (NWF) and northeast (NEF) of the central zone. Micro-meteorological sensors measured energy and water fluxes at a semi-hourly time step. They were: (i) net radiometers and eddy correlation systems installed on towers at a 2-m height; and (ii) soil moisture probes put in soil pits. This equipment was installed from 17 December 2007 to 17 May 2008 on NWF and from 30 December 2007 to 10 May 2008 on NEF. Net radiations were measured using a CNR1 (Kipp & Zonen Inc., Delft, The Netherlands) and a Q6 (Campbell Scientific Inc., Logan, UT, USA) on the NEF and NWF sites, respectively. Sensible heat fluxes were monitored through the eddy correlation technique using high-frequency 3D sonic anemometers (CSAT3, Campbell Scientific Inc., Logan, UT, USA). Net radiation and sensible heat fluxes were accumulated every 24 h to obtain daily values. Daily latent heat flux was computed from the residual of the surface energy balance as the difference between net radiation and sensible heat flux. We assumed here that both the soil heat flux and the canopy heat storage are negligible. This assumption is not critical at the daily time step on homogeneous bare soil and short crops [46,47]. Daily latent heat fluxes were divided by the latent heat of vaporization to obtain evapotranspiration in $mm \cdot day^{-1}$ (more details can be found in [48]). Soil moisture was measured every 30 min by water content reflectometers (CS616 probes, Campbell Scientific Inc., Logan, UT, USA), which were set up within soil pits at 5- and 30-cm depths. These measurements were transformed in volumetric soil humidity after calibration against moisture derived from soil samples using the gravimetric approach. Daily averaged values were used in this study.

Agricultural practices were collected on 40 wheat fields located in the central zone. Sowing and irrigation dates were used in this study. The sowing period ranged from 25 November 2007 to 8 January 2008, with a systematic pre-irrigation before the seedling. After sowing, there were 3 to 4 irrigations for wheat crops. Furrow irrigation was used, with a water quantity estimated around 150 mm each irrigation. These are common practices in the Yaqui Valley [42].

The vegetation biophysical variables are Green Leaf Area Index (GLA, in $m^2 \cdot m^{-2}$) and grain yield (GY, in $t \cdot ha^{-1}$). GLA was derived from hemispherical photography taken on 20 × 20 m^2 sampling units according to the VALERI protocol [49]. The processing of hemi-views was based on the analysis of the canopy directional gap fraction following the procedure designed by [50]. Harvests occurred from the end of April until mid-June, 2008. GY was obtained by surveying harvesting machines with a GPS device operating in track mode. This survey was achieved on 11 fields located in the northern part of the central zone (Figure 1). Grain yield was calculated as the (dry) weight of grain collected by harvesting machines divided by the harvested surface, the latter being estimated by analyzing GPS records.

Soil properties were derived from field measurements performed on 13 plots sampled within the central zone using a auger. Humidity at field capacity and the wilting point were estimated from the soil texture based on the pedotransfer approach [51,52]. The texture was derived from soil samples for the 0 to 20 cm and the 20 to 40 cm soil layers. Soil texture was on average 43.5% clay, 36.5% sand and 20% silt. It was found to be homogeneous within the study area, both vertically and horizontally. Therefore, a unique value was computed by applying the pedotransfer function of [53]. These measurements also showed no limitations on soil depth without the observation of parent materials until 1 m.

2.3. FORMOSAT-2 Images

The FORMOSAT-2 Taiwanese satellite, launched in May 2004, provides 8-m spatial resolution images in four narrow spectral bands ranging from the blue (0.45 μm) to the near-infrared (0.90 μm) part of the electromagnetic spectrum. Unlike other systems operating at decametric resolution, FORMOSAT-2 may observe a particular area every day with the same viewing angle. More details about the specific orbital cycle and other characteristics of the FORMOSAT-2 mission could be found in [28], as well as on the Internet [54,55].

The images were acquired over the study area and its 24 × 24 km^2 surroundings with a constant view zenith angle about 12°. Acquisitions were programmed from 15 November 2007 to 6 June 2008 with a nominal time step of 5 days. There was almost no cloud during the satellite overpasses, and the maximal lag between two acquisitions was 10 days. A unique dataset of 36 FORMOSAT-2 images encompassing the 2007 to 2008 wheat growing season was collected (Figure 2).

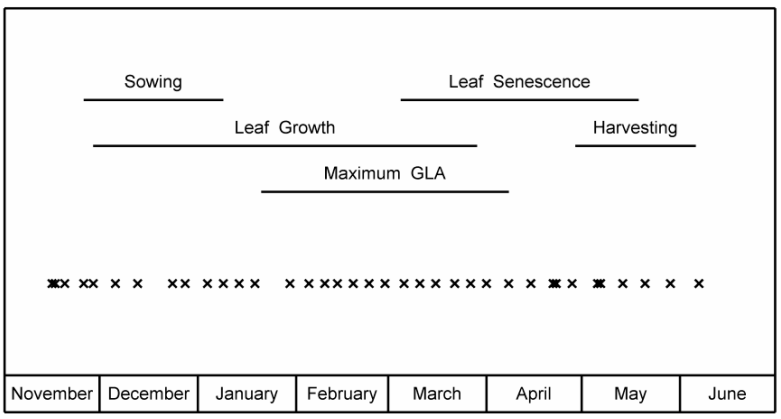

Figure 2. *Cont.*

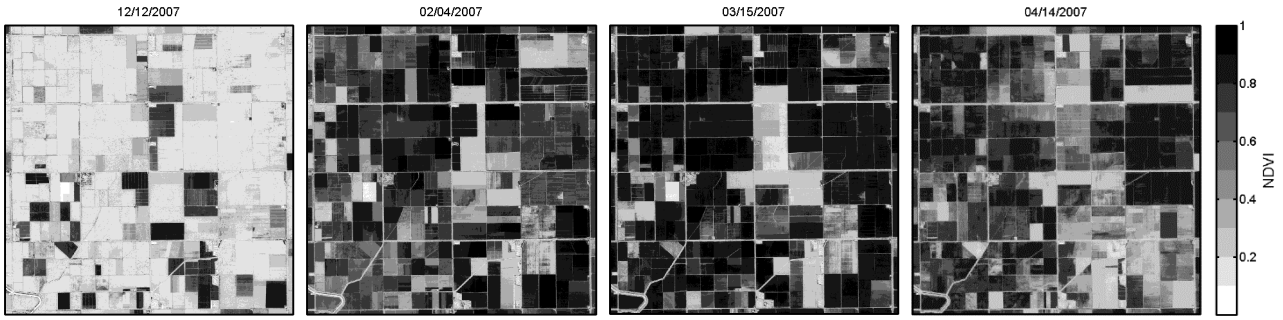

Figure 2. FORMOSAT-2 acquisition dates (×) together with the main agricultural operations and phenological phases for wheat crops (GLA, Green Leaf Area) and examples of NDVI images.

The images were superimposed through a cross-correlation technique and georeferenced in the UTM 12N projection system based on a set of GPS ground control points. Accuracy in the geolocalization was estimated to about a half-pixel (4 m). The atmospheric correction was performed using the Simplified Method for Atmospheric Correction (SMAC) code [56] with an original method developed for the retrieval of aerosol optical thickness using constant values of atmospheric water vapor and ozone contents [29]. Finally, the Normalized Difference Vegetation Index (NDVI, [57]) was computed as the ratio of the difference between near-infrared and red reflectances from their sum.

2.4. The SAFY-WB Model

Simulations were performed using the Simple Algorithm For Yield estimates (SAFY) vegetation growth model [58] coupled to a water balance (WB) model adapted from the FAO-56 method [59,60]. This coupling results in the SAFY-WB model, which simulates the daily time courses of the Total and the Green Leaf Area Indexes (TLA, GLA), the dry aboveground mass (DAM), the evapotranspiration (ET) and the soil water content (SWC) in three different soil layers (top, intermediate, deep). The inputs of the model are daily values of the incoming global radiation (Rg), the air temperature (Tair), the reference evapotranspiration (ETo), precipitation (P) and irrigation (I). Irrigation can be prescribed as an input of the model (forced mode) or repeatedly activated when a critical value of the soil water content is reached (automatic mode).

2.4.1. Vegetation Growth

We used the SAFY model, which has been fully described in [57]. Only the basic processes and formalisms are presented. The SAFY model simulates the daily variations of Leaf Area Index (GLA and TLA) and dry matter (DAM) from the day of plant emergence to the day of total plant senescence. DAM production is proportional to the absorbed photosynthetically-active radiation (APAR) according to the effective light-use-efficiency (adapted from [61]). The photosynthetically-active fraction of solar radiation absorbed by plants is a logarithmic function of GLA (Beer–Lambert law, [62]). Two main phenological phases are controlled by growing degree-day: leaf production and leaf senescence. During the leaf production phase, the fraction of the daily DAM production partitioned to the leaf depends on the accumulated temperature based on the empirical parameterization proposed by [63]. The

senescence occurs at a prescribed rate, when the air temperature accumulated from plant emergence reaches a given threshold. Air temperature also affects DAM production through a temperature-stress-function based on 2-degree polynomials specified by an optimal value (20 °C) and two extreme values (0 °C and 37 °C) beyond which the wheat growth stops [64,65].

The SAFY model has been already applied to wheat, maize, sunflower and soybean crops [34,58,66,67]. In this study, it was applied with the parameterization adapted to winter wheat crops in Central Morocco presented in [58], except two parameters: one parameter in the empirical parameterization used to partition biomass to leaf (Pla, set to 0.2) and the threshold that controls the start of senescence (set to 1440 °C).

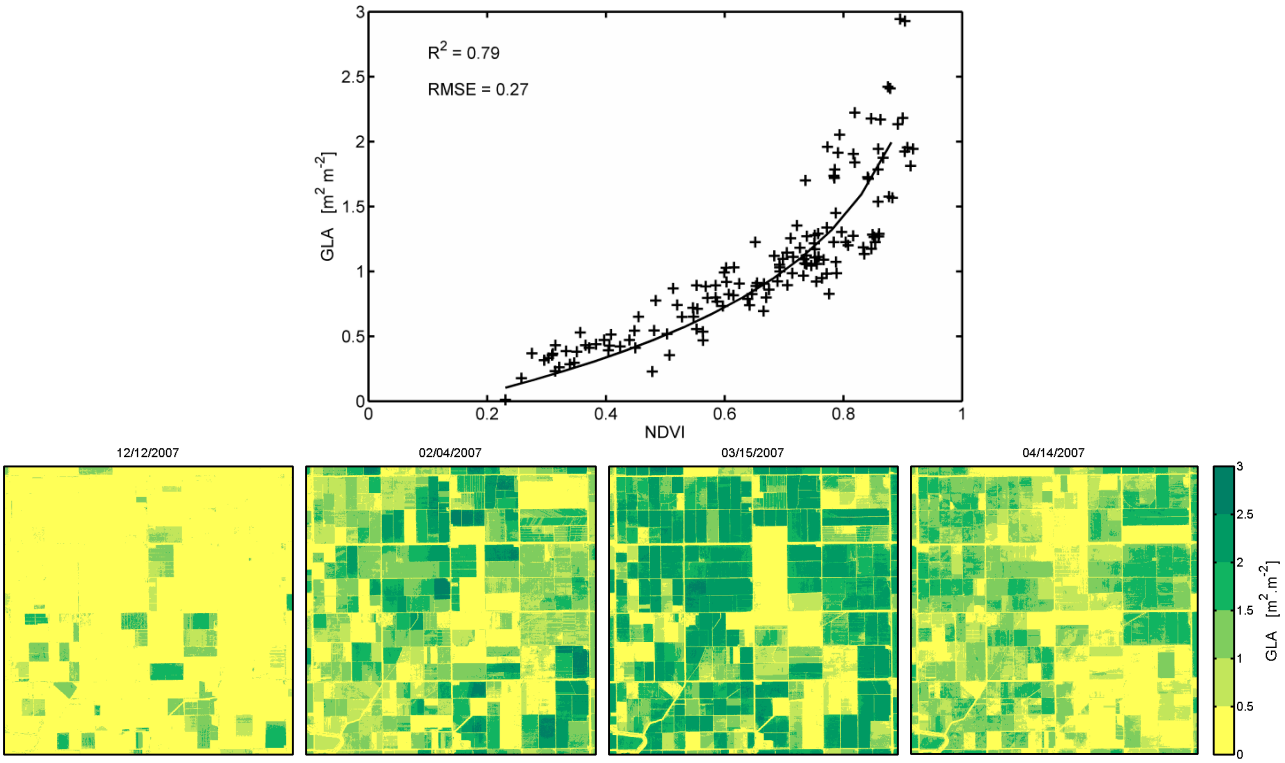

Figure 3. Relationship between the Normalized Difference Vegetation Index (NDVI) and the Green Leaf Area Index (GLA), together with examples of GLA images. The determination coefficient and the root mean square error associated with the logarithmic relationship are indicated.

The key variable of the SAFY model is GLA, which was mapped from each FORMOSAT-2 datum using a fully-empirical method. The NDVI-GLA relationship was established between *in situ* GLA data derived from hemi-views and NDVI averaged over 3 × 3 pixels centered on the 20 × 20 m^2 sampling units where the photography was taken. The NDVI shows a logarithmic response to GLA (Equation (1) and Figure 3), in agreement with the results obtained in previous studies (e.g., [68–70]). The empirical relationship between NDVI and LAI is associated with acceptable statistical indexes, a determination coefficient R^2 of 0.79 and an RMSE of 0.27 $m^2 \cdot m^{-2}$ (25% in relative value). This relationship was used to derive GLA from FORMOSAT-2 images throughout the entire agricultural season. Time series of GLA were used to adjust two parameters of the SAFY model: the day of plant emergence and the effective light use efficiency. This is described in what follows (Section 2.5).

$$GLA = -\log((NDVI_{inf} - NDVI)/(NDVI_{inf} - NDVI_{sol})) \times 1/k \quad (1)$$

where $NDVI_{inf}$, $NDVI_{sol}$ and k are empirical parameters equal to 0.97, 0.14 and 1.12, respectively.

2.4.2. Water Balance and Evapotranspiration

The water balance model simulates the water transfer mechanisms between two or three different soil layers (gravity and diffusive fluxes) and between the soil and the atmosphere (evaporation and transpiration). The soil depth was fixed to 1.5 m. Out of the growing period, the soil is split into two layers, a 10-cm depth top layer providing water for evaporation and a deep layer. During the growing period, an intermediate layer is delimited by the root front. The depth of the root front is set to 20 cm at plant emergence, and then, it increases until the end of leaf production to a maximal value of about 1 m. The root zone, where the water is extracted for transpiration, corresponds to the top and the intermediate layers.

The soil properties are also described by humidity at field capacity (H_{fc}) and at the wilting point (H_{wp}), which have been estimated by applying the pedotransfer function of [53] as 0.39 and 0.26 $m^3 \cdot m^{-3}$, respectively. Each soil layer is characterized by: (i) its current available water content (CAW_x), which is updated every day according to inflows and outflows; and (ii) its storage capacity (SC_x; Equation (2)), which is computed according to the thickness of the layer (SLT_x) and the difference between humidity at field capacity and at the wilting point. Drainage by gravity (D_x; Equation (3)) is effective after rain or irrigation when the water content in the layer is greater than its storage capacity.

$$SC_x = (H_{fc} - H_{wp}) \times SLT_x \quad (2)$$

$$D_x = \max[SC_x - CAW_x, 0] \quad (3)$$

where x corresponds to the top (t), the intermediate (i) or the deep (d) soil layer.

In addition to gravity fluxes, the soil water content is updated to account for capillary rise. The formalism was adapted from [71]. The diffusive flux between two adjacent layers x and y ($\Phi_{x/y}$; Equation (4)) is a linear function of the difference of humidity between the two layers ($H_x - H_y$) normalized by the humidity at field capacity. It is applied either between the top and the deep layers (out of the growing season) or, successively, between the top and the intermediate layers and between the intermediate and the deep layers (during the cropping season).

$$\Phi_{x/y} = 0.27 \times [(H_x - H_y)/H_{fc}] \quad (4)$$

where x and y refer to two adjacent soil layers.

Evapotranspiration (ET; Equation (5)) is calculated according to the FAO-56 method [59,60] from the reference evapotranspiration (ETo) and two coefficients Ke and Kt that simulate the rate of soil evaporation (E) and of plant transpiration (T), respectively. ETo is derived from climatic parameters, according to the Penman–Monteith equation adapted for a hypothetical grass reference surface. The calculation was performed using daily values derived from half-hourly measurements of the incoming solar radiation, the air temperature, the wind speed, the relative humidity and the atmospheric pressure, in accordance with the standardized equations given in [72] and [59–73].

$$ET = E + T = [Ke + Kt] \times ETo \quad (5)$$

Soil water evaporation (E; Equation (6)) is calculated by multiplying the reference crop evapotranspiration (ETo) and the soil water evaporation coefficient (Ke; Equation (7)). Evaporation is reduced according to the reduction coefficient that limits evaporation when the soil dries up (Kr in Equation (7)) and to the fraction of the soil covered by the vegetation (FC; Equation (8)). Kr is computed from the top soil relative humidity using a bilinear function (Equation (74) and Table 19 in [59]). It is set to 1 if the top soil relative humidity is greater than 50%; then, it decreases linearly to 0 when the soil is totally dry. The vegetation fraction cover (FC; Equation (8)) is simulated from the value of the Green and the Total Leaf Area Indexes using an empirical formalism, which has been adjusted from *in situ* data.

$$E = Ke \times ETo \tag{6}$$

$$Ke = (1 - FC) \times Kr \tag{7}$$

$$FC = 0.95 \times (1 - e^{-0.53 \times TLA}) \times (GLA + TLA)/(2 \times TLA) \tag{8}$$

Transpiration (T; Equation (9)) is calculated during the growing season from the reference crop evapotranspiration ETo and a transpiration coefficient. T is null outside the growing season. The transpiration coefficient (Kt; Equation (10)) is the product of a water stress coefficient (Ks) and of the basal crop coefficient (Kcb). Kcb relies on plant maximal transpiration and varies according to the crop type and development stage. It is derived from GLA using the exponential relationship set up by [70] for wheat crops in Central Morocco (Equation (11)). The water stress coefficient (Ks) is derived from the relative humidity of the soil layer, considering the higher value between the top and the intermediate layers. As for the calculation of the soil evaporation reduction coefficient, the stress function is bilinear, varying from 0 to 1 below the critical humidity point, which was set to 40% (Equation (84) and Table 22 in [59]). In other words, it is simply assumed that plants do not suffer from water stress if the relative humidity of either the top or the intermediate layer is greater than 40%.

$$T = Kt \times ETo \tag{9}$$

$$Kt = Ks \times Kcb \tag{10}$$

$$Kcb = 0.92 \times (1 - e^{-0.84 \times GLA}) \tag{11}$$

During the period of simulation, the soil water content in each layer is updated daily according to the inflows and the outflows previously described. The available water in the top soil layer (CAW_t; Equation (12)) is updated from the effective rainfall (REF), irrigation (I), soil evaporation (E), plant transpiration (T), gravity (D_t) and diffusive ($\Phi_{t/y}$) fluxes between the top and the deeper layer (y). The effective rainfall (REF; Equation (13)) is computed from daily rainfall (R) with an account of: (i) the interception by the canopy, through its Total Leaf Area Index (TLA); and (ii) the evaporative demand, through the reference evapotranspiration (ETo). This formalism was adapted from [74]. Evaporated water depletes the top layer, while transpired water depletes both the top and the intermediate layer, *i.e.*, the root zone. The fraction of the transpired water extracted on the topsoil (tpf in Equation (12)) is the ratio of the current available water between the topsoil and the intermediate layer. It is simply assumed that the plant takes the water preferentially where it is. Gravity and diffusive fluxes are applied between the top and the deep layers out of the growing season and between the top and the intermediate layers during the growing season. Gravity fluxes are effective

when the current available water exceeds the layer's storage capacity (see Equation (3)). The water overload is drained to the deeper layer.

$$CAW_t \leftarrow +REF + I - E - tpf \times T - D_t \pm \Phi_{t/y} \quad (12)$$

where t corresponds to the top layer and y refers to either the intermediate or the deep soil layer (the arrow means that the left variable is updated from one day to the next according to the variables and operations listed in the right part of the equation).

$$REF = R - \max[R \times (1 - 0.5^{TLA}), ETo]) \quad (13)$$

During the growing season, the available water in the intermediate soil layer (CAW_i; Equation (14)) is balanced by the drainage from the top soil layer (D_t) and to the deep layer (D_i), the part of transpirated water (T) that is not taken from topsoil (1 − tpf) and the diffusive fluxes exchanged with the top ($\Phi_{t/i}$) and the deep layer ($\Phi_{i/d}$). This leads to:

$$CAW_i \leftarrow + D_t - D_i - (1 - tpf) \times T \pm \Phi_{t/i} \pm \Phi_{i/d} \quad (14)$$

where t, i and d correspond to the top, the intermediate and the deep layer, respectively.

Finally, the available water in the deep soil layer (CAW_d; Equation (15)) is updated depending on the gravimetric and the diffusive fluxes ($\Phi_{x/d}$) exchanged with the upper layer (x). When the relative soil moisture of the deep layer exceeds that of the upper layer, water can go up by capillary rise. If the drainage is larger than the difference between the layer storage capacity and its available content, the water surplus (D_d; see Equation (3)) is removed and definitively lost for the soil-plant system.

$$CAW_d \leftarrow + D_x - D_d \pm \Phi_{x/d} \quad (15)$$

where d corresponds to the deep layer and x refers to either the top or the intermediate layer.

In order to be compared with field measurement, the volumetric soil moisture (in $m^3 \cdot m^{-3}$) was derived from the soil water content and the soil bulk density.

2.5. Model Setup

To perform simulations over the whole study area, 528 fields were regularly delineated, each covering 5 ha. This delineation was performed using an automatic segmentation algorithm to split large fields into smaller ones sized 100 m across the row direction and 500 m along the row direction, 100 m being the length that can be irrigated in one day. These units thus correspond to homogenous spatial units, both in terms of vegetation dynamics and agricultural practices (same sowing and irrigation days). Time series of GLA derived from FORMOSAT-2 images were built by simple averaging on each field.

The SAFY model was set up according to the parametrization described in the previous section, except two parameters—the day of plant emergence and the effective light-use efficiency—which were adjusted by comparing the time series of GLA simulated by SAFY and those derived from FORMOSAT-2 images. This procedure was applied successively and independently on each field by minimizing the difference between simulated and remotely-sensed GLA using the root mean square error as a cost function.

After this calibration, the SAFY-WB model was run under two irrigation modes. The first was a "forced mode", where we used the exact dates of irrigation and quantity of water observed at the field

to simulate actual evapotranspiration and soil water content (AET, SWC). This mode was set up on the NWF and NEF sites where micrometeorological measurements were collected. The comparison of simulations and measurements allowed testing the performance of the water balance model. The second was an "automatic mode", where we used the automatic mode on each of the 528 fields. In this case, irrigations were activated according to the value of the plant water stress function or, equivalently, to the soil water content of the root zone. The analysis of irrigation data showed that a large quantity of water is supplied during the agricultural season, at least 600 mm for the wheat fields located in the central zone. This value corresponds to well-watered wheat crops [75] and is much larger than wheat crop seasonal evapotranspiration, which is about 400 mm, as estimated by [76]. Therefore, we have applied a rule to fulfill crop water requirements, activating irrigation as soon as the plant stress coefficient (Ks in Equation (10)) was below 1. The water amount for each irrigation was fixed to the mean value observed in the central zone (150 mm).

In each mode, the period of simulation ranged from 1 September 2007 to 31 May 2008. The soil was initialized as it was totally dry. A pre-irrigation is applied during November one month before the day of sowing. This delay corresponds to what has been observed from the agricultural operations recorded in the central zone.

2.6. Water Use Efficiency

Water use efficiency (WUE) can be defined at different spatial (watershed, irrigated area, farm, field, plant) and temporal (daily, weekly, seasonal, yearly) scales [18–20]. In it most general sense, WUE refers to the ratio of the amount of water supplied to achieve a given output. In agricultural sciences, both the "type" of water whose use is being optimized (rainfall, irrigation, transpired or drained water, *etc*.) and the type of output (grain, tuber or fruit yield, total dry matter, *etc*.) may vary according to the process that is being optimized and the objective of the optimization. There are thus many possible ways to define WUE.

In this paper, WUE is estimated on a seasonal basis as the ratio of the accumulated dry aboveground mass divided by the seasonal evapotranspiration. WUE was derived on each field from two outputs of the SAFY-WB model: the (maximal value of the) dry aerial biomass simulated at the end of the growing season and daily values of evapotranspiration, which were accumulated from the day of plant emergence to the day of total plant senescence. It should be noted that this definition of WUE corresponds to that mentioned in the Introduction for the agronomical approach [7], except that the root mass is not considered in the calculation and that the period used to calculate the water consumption is not the whole cropping season, from pre-irrigation to harvesting, but the growing season. Furthermore, seasonal evapotranspiration meant the total water that is evapotranspired over the entire growing season, and it includes rainfall and irrigation water, *i.e.*, the applied water. As rainfall (32 mm between November 2007 and May 2008) was negligible compared to irrigation (at least 600 mm), the WUE calculated in this study is almost an irrigation water use efficiency. Last, both soil evaporation and plant transpiration is considered in the calculation of WUE. We are not optimizing the "effective use of water" [26], which would imply maximizing either the rate of biomass production per transpired water or the soil moisture capture for transpiration (thus minimizing water loss by soil evaporation). The issue addressed here is identifying the adequate sowing period for increasing wheat

yield cultivated under furrow irrigation practices, not to compare the performance between species or between irrigation techniques.

3. Model Evaluation

3.1. Vegetation Growth

The model evaluation is based on data acquired at different scales: the Green Leaf Area Index derived from FORMOSAT-2 images over the whole 8 × 8 km^2 study area; the sowing date collected on wheat fields located in the central zone; and the grain yield measured on the northern part of the central zone (see Figure 1).

Firstly, we have compared the GLA values simulated by SAFY at the time of FORMOSAT-2 overpasses and those derived from FORMOSAT-2 images (Figure 4). Considering all simulations and observations (19,008 paired values crossing 36 dates and 528 fields), GLA was reproduced by the SAFY model with a very high determination coefficient (R^2 = 0.98) and without any bias (Figure 4a). We also have calculated the relative root means square error (rRMSE) associated with the time courses of GLA successively simulated for each of the 528 fields over the 8 × 8 km^2 study area. The analysis of the frequency histogram (Figure 4b) showed that rRMSE was: (i) 12% on average; (ii) lower than 20% for 95% percent of the wheat fields; and (iii) 26.5% at maximum. This range of error appears quite acceptable with regard to the accuracy of field GLA measurements [49,77]. However, this good result cannot be considered as a validation, as time series of GLA were used to calibrate the SAFY model. This comparison just confirms that the SAFY model is a good interpolator of GLA. This conclusion was also stated from previous experiments on wheat crops [34,58,67], as well as on maize, soybean and sunflower crops [66].

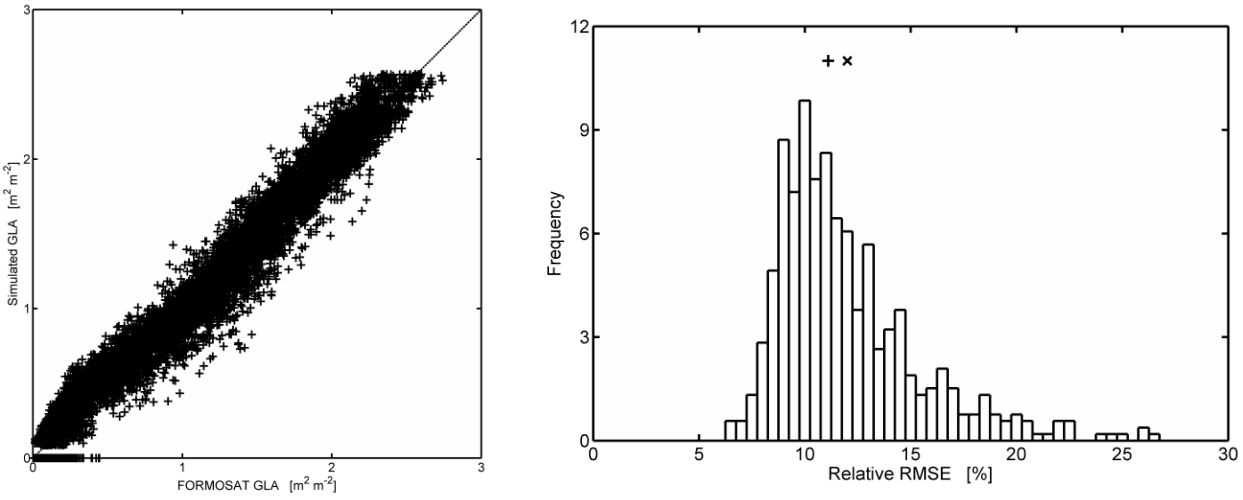

(**a**) (**b**)

Figure 4. (**a**) Scatterplot between values of the Green Leaf Area Index (GLA) simulated by SAFY and derived from FORMOSAT-2 time series data. The dotted line highlights the X = Y line. (**b**) Frequency histogram of relative RMSE on simulated GLA. Symbols indicate the median (+) and the mean (×) values.

Secondly, we have compared the sowing dates collected on 40 wheat fields located in the central zone with the days of plant emergence retrieved after the calibration of the SAFY model (Figure 5). The global agreement between these two variables was high (R^2 ~0.86, slope of 1.02). The time lag between sowing and emergence appeared very regular, about 10 days for a large majority of the fields. This regularity was expected, since the soil moisture is controlled by pre-irrigation; there was thus no hydric constraint for seeds germinating. The density of FORMOSAT-2 observations makes us confident in these estimates in contrast to the studies based on a reduced number of satellite observations (e.g., [39,78,79]).

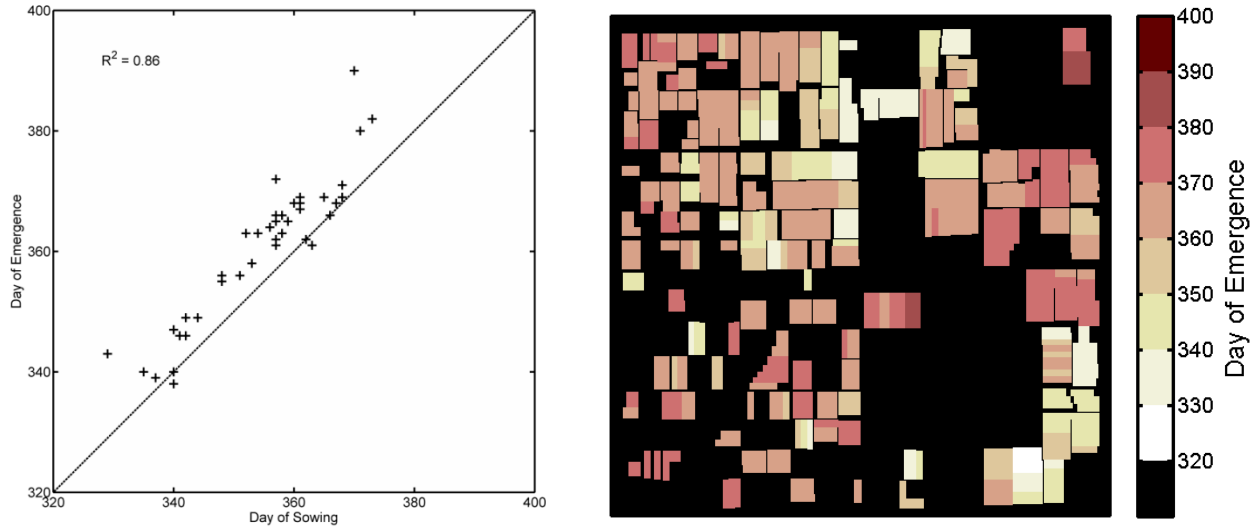

Figure 5. Comparison between sowing and emergence dates for wheat fields where agricultural practices were collected (dates are in number of days after the 1 January 2007). The dotted line is the X = Y line (**left**). Spatial patterns of the day of emergence (**right**).

Lastly, the evaluation of DAM simulation was performed using the grain yield measurements available for the 11 fields where the harvesting was monitored (Figure 6). On these fields, the dry aerial mass simulated at the end of the season varies between 9.5 and 13.5 $t \cdot ha^{-1}$, while the grain yield observed at the field ranges between 4 and 8 $t \cdot ha^{-1}$. The two variables were found to be very well correlated (R^2 ~0.91). This strong association between grain yield and biomass production was already pointed out by [80] for various wheat cultivars in the Yaqui Valley during a two-year experiment (1995 to 1997). The difference between grain yield and total crop production is on average 5 $t \cdot ha^{-1}$. The corresponding harvest index (HI), calculated as the ratio of the grain yield-to-the total crop production, is 0.52 (min = 0.41, max = 0.61, std = 0.065). Considering grain moisture of about 18% at harvesting time (after [81]), the 0% moisture harvest index was on average 0.43. This value appeared correct for wheat crops cultivated within the Yaqui Valley: [82] have reported values between 0.35 and 0.44 during the 1993 to 1994 and the 1994 to 1995 seasons; [83], cited by [76], have conducted 24 trials on wheat in Yaqui from 1999 to 2000, for which the average HI was 0.42 (with a standard deviation of 0.04); HI values between 0.36 and 0.39 have also been derived by [39] from 80 different fields from 2000 to 2001.

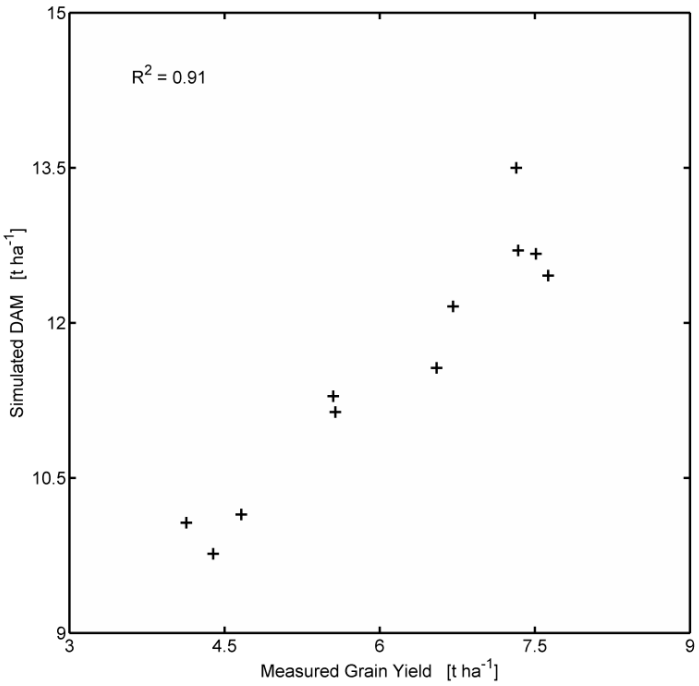

Figure 6. Dry aboveground biomass (DAM) simulated by the SAFY-WB model *versus* grain yield measured at the field.

3.2. Water Balance

Simulations of evapotranspiration (ET) and soil moisture (SM) were evaluated against the variables derived from the two micrometeorological stations installed on NWF and NEF. The SAFY-WB model was run two times in the forced irrigation mode considering sites of 3 ha (21 × 21 FORMOSAT-2 pixels) centered on each of the stations. The size of the sites is compatible with the footprint of ET measured through the eddy correlation technique [84]. Each of the two sites is homogeneous in terms of agricultural practices (same sowing and irrigation days) and vegetation development (low GLA variability). The analysis of the irrigation schedules showed that after pre-irrigation and seedling, NWF was irrigated four times and NEF was irrigated three times, supplying 150 mm of water each time.

Figure 7 displays the time courses of the actual (AET) and the reference (ETo) evapotranspiration on the two sites. The growing season could be clearly identified by both estimated AET (AET_{est}) and measured AET (AET_{mes}). AET_{est} progressively increased from about 1 mm·d^{-1} at plant emergence (Day 353 on NWF, Day 342 on NEF) to a value close to ETo when the canopy was recovering the soil (fraction cover (FC) of 0.5 for Day 409 on NWF, Day 398 on NEF); then, it decreased during the senescence phase (Days 446 to 491 on NWF, Days 437 to 485 on NEF). The seasonal evapotranspiration, *i.e.*, daily values accumulated from the day of plant emergence to the day of plant total senescence, were 412 mm and 455 mm for NWF and NEF, respectively.

The cross-comparison of the time courses of AET_{mes} and ETo in Figure 7 is also instructive to detect periods of plant water stress. These two variables displayed coherent covariation, with no sharp discrepancies between AET_{mes} and ETo, whatever the irrigation status. Furthermore, the ratio between AET_{mes} and ETo is inferior to the crop coefficients displayed by [59], for non-stressed crops. This confirmed that wheat plants have not suffered from severe water stress [70,85].

There is also a high agreement between simulated and measured ET in Figure 7: the bias is 0.55 mm for NWF and 0.03 for NEF; the relative root mean square error (rRMSE) between these two variables is 24% for NWF and 22% for NEF; the determination coefficient (R^2) is 0.88 for NWF and 0.72 for NEF. Simulations and observations appeared comparable across the entire growing season, except on NWF for the period before Day 397, during which simulations underestimated measurements. Measured ET appeared unrealistically low in this period, and it is probable that measurement problems occurred at the beginning of the experiment. Simulated ET appeared underestimated, and the soil drying appeared overestimated on the NEF site during the senescence phase. Despite this period of discrepancy, ET simulations appeared of better quality compared to those performed by [37] using the complex STICS crop model (Simulateur mulTIdisciplinaire pour les Cultures Standard). The accuracy of simulations appeared also comparable to remote sensing estimates provided by the SEBAL model (Surface Energy Balance Algorithm for Land) in the same area [76].

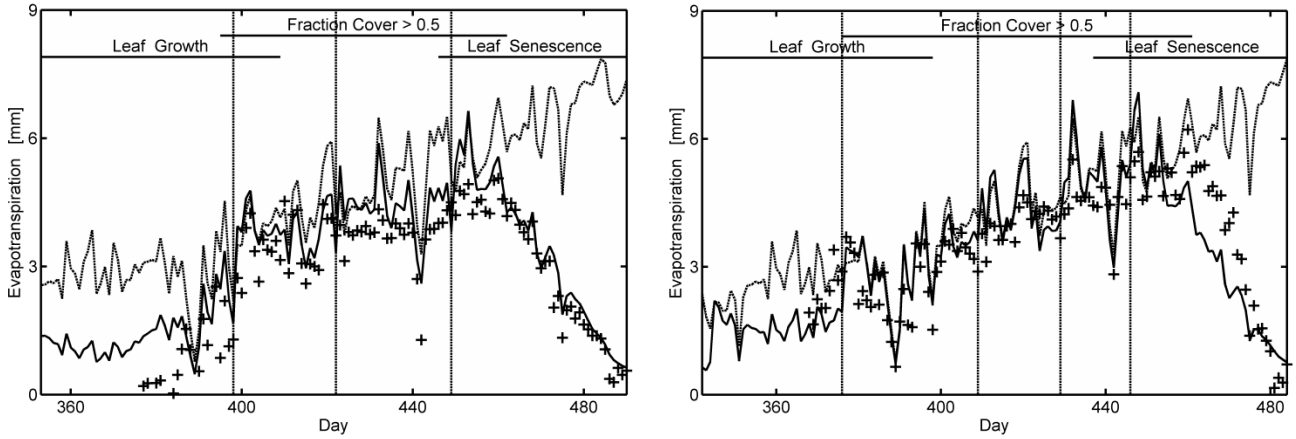

Figure 7. Times courses of measured (AET_{mes}, stars), estimated (AET_{est}, full lines) and reference evapotranspiration (ETo, dotted lines): northwest field (NWF) (**left**), northeast field (NEF) (**right**). Vertical lines highlight irrigation events. The days are numbered from 1 January 2007.

The dynamics of the soil water content (SWC) also appeared well simulated by the SAFY-WB model (Figure 8). The model was able to reproduce the peaks and the drying phases associated with successive irrigations, three times on NWF and four times on NEF. Both simulated and observed soil moisture reached field capacity just after an irrigation day, then decreased to reach the wilting point just before the next irrigation day. However, the model seemed to overestimate top-soil drying on NEF (Figure 8, top-right). The possible explanations are: (i) the use of a single value of wilting point humidity in simulations, which is derived from soil analysis with a limited sampling scheme; and (ii) the representativeness and accuracy of soil moisture measurements. This overestimation explained why ET is underestimated during the senescence phase (Figure 7, right). The performance of the model to simulate the time courses of soil humidity after rainfall was also remarkable. This was verified both for low rainfall that only supplied the topsoil layer (7 mm on Day 389; Figure 8, top) than for the moderate rainfall that affects both the top and the intermediate soil layers (25 mm on Day 344; Figure 8, right).

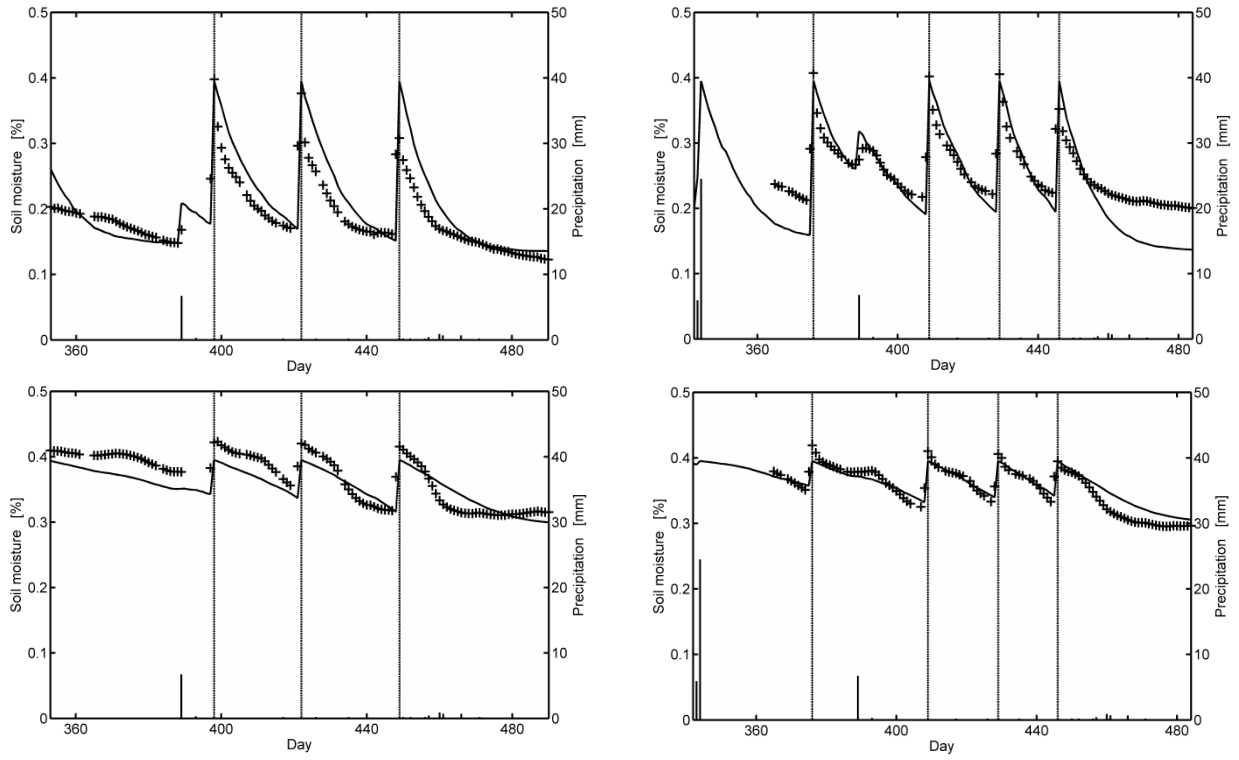

Figure 8. Times course of measured (stars) and simulated (lines) volumetric soil water content. The left and right figures display the results obtained on NWF and NEF fields, respectively. The top figures display the results obtained for soil moisture for the top and intermediate soil layers, respectively. Vertical lines highlight irrigation events. The days are numbered from 1 January 2007.

Simulations of SWC were quantitatively evaluated using the data collected from water content reflectometers. The 5-cm depth measurements were compared to simulations obtained for the 10-cm top soil layer (Figure 8 top): R^2 and rRMSE between simulated and measured top soil moisture were 0.78 and 20% on NWF and 0.83 and 16% on NEF. Measurements collected at 30-cm depths were compared to SWC simulated on the intermediate soil layer (Figure 8, bottom), the latter being bounded by the top soil layer (10-cm depth) and the root front (20-cm depth at plant emergence to about 1 m after that GLA reached is maximal value). R^2 and rRMSE between these two variables are 0.79 and 6% on NWF and 0.91 and 4% on NEF. These performances appeared quite satisfactory keeping in mind that soil water content is measured using probes installed at single points (geolocation and depth), whereas simulations correspond to a much larger area, both horizontally (3 ha) and vertically (10-cm to 1-m soil layers).

3.3. Irrigation Modes

The outputs of SAFY-WB runs obtained with automated irrigations were evaluated at the NWF and NEF sites by comparison with the previous simulations obtained with actual irrigation schedules. In the automatic mode, a 150-mm water irrigation was supplied every time the crops started to suffer from a water stress, *i.e.*, when the plant water stress coefficient (Ks in Equation (10)) became lower than one. We first verified that there was no difference in the vegetation biophysical variables between

the two modes. This was expected, since no stress was observed on the plants within NWF and NEF (see Figure 8), which were abundantly irrigated (600 and 750 mm when including irrigation operated before sowing). After this, the comparison of the variables related to the water balance between the two irrigation modes showed that: (i) the number of irrigations was three on both fields in the automatic mode; this was the same as what was observed at the field on NWF, but less by one on NEF; (ii) on NWF, the seasonal evapotranspiration obtained in the forced mode (412 mm) was similar to that obtained in the automatic mode (415 mm); in this case, the number of irrigations post-sowing was three; and (iii) on NEF, the seasonal evapotranspiration was slightly greater in the forced mode with four irrigations (455 mm) than in the automatic mode with three irrigations (443 mm).

4. Crop Production, Seasonal Evapotranspiration and Water Use Efficiency

This previous analysis showed that seasonal evapotranspiration simulated on NWF and NEF by the SAFY-WB model slightly differed between actual and automated irrigations. It is thus suggested that evapotranspiration simulated with the automatic irrigation mode was suitable for calculating the water use efficiency on well-watered fields. This last condition appeared satisfied for the 4 × 4 km^2 central zone where at least 600 mm was supplied by irrigation (see Section 2.5). We assumed that it is still valid over the whole 8 × 8 km^2 study area. The model was run for each of the 528 fields of the 8 × 8 km^2 study area using automated irrigation.

We were mainly interested in the spatial variations of three outputs—crop production, seasonal evapotranspiration and water use efficiency—in relation to the day of plant emergence derived from time series of remotely-sensed GLA and model calibration, which was found to vary from 23 November 2007 (Day 327) to 24 January 2008 (Day 389) over the whole study area. Before discussing this, we focused on two representative wheat crops cultivated under early sowing (ES) and late sowing (LS). Figure 9a,b displays the time courses of key biophysical variables on two fields where the plant emergence days were Day 338 (ES) and Day 368 (LS), respectively. The comparison of the two figures allowed illustrating that the growing season is longer for ES (144 days) than for LS (133 days), and the maximal GLA was much larger for ES (2.5 $m^2 \cdot m^{-2}$) than for LS (1.8 $m^2 \cdot m^{-2}$). Consequently, the photosynthetically-active radiation absorbed by the canopy (APAR) was higher for ES (680 $MJ \cdot m^{-2}$) than for LS (587 $MJ \cdot m^{-2}$), as well as the crop production, with an accumulated DAM reaching 13.9 $t \cdot ha^{-1}$ for ES against 9.5 $t \cdot ha^{-1}$ for LS. Evapotranspiration was reduced for LS compared to ES at the beginning of the season during 73 days with moderate reference evapotranspiration (days before 410, ETo averaged 338 to 410 = 2.9 $mm \cdot d^{-1}$, sum = 211 mm); then, it is roughly similar on the two fields, close to ETo (Days 410 to 460); then, it is reduced for ES compared to LS during 40 days with a high evaporative demand (days after 460, ETo averaged 460 to 500 = 6.9 $mm \cdot d^{-1}$, sum = 283 mm). Consequently, the seasonal evapotranspiration is almost the same on the two fields, 444 mm for ES and 422 mm for LS.

Figure 10 presents the covariation between the day of plant emergence (DoPE) and the crop production (DAM). It is visible that these two variables were correlated. The trend previously illustrated in Figure 9 was conserved: DAM decreased about 15 $t \cdot ha^{-1}$ for the fields sown the earliest (DoPE around 330) to 6 $t \cdot ha^{-1}$ for the fields sown the latest (DoPE around 380). There is a sharp decrease in crop production for the majority of the fields sown the latest that experienced reduced plant

development (GLA never exceeds 1.5; circles in Figure 10) and, thus, reduced PAR absorption. A deeper analysis of these simulations shows that the explanations stated in the two particular examples previously presented were preserved: late sowing resulted in a decrease of both the length of the growing season and the plant development (maximal GLA), thus in a reduced absorption of photosynthetically-active radiation and biomass production. This result is coherent with the statement of the previous modeling experiment of [37] performed using data collected on 16 wheat fields in the Yaqui Valley during the 1999 to 2000 agricultural season. In this study, most of the fields that were sown before 11 December experienced a high yield between 6 and 7 $t \cdot ha^{-1}$, whereas two fields sown after 17 December experienced a lower yield around 4.5 $t \cdot ha^{-1}$. The work in [86], who conducted research concerning wheat yield and nitrogen use efficiency at the CIANO (Centro de Investigaciones Agricolas del NorOeste) research center near Ciudad Obregon during eight seasons from 1997 to 1998 to 2004 to 2005, reported that "sowing always occurred during the optimum late November to early December period".

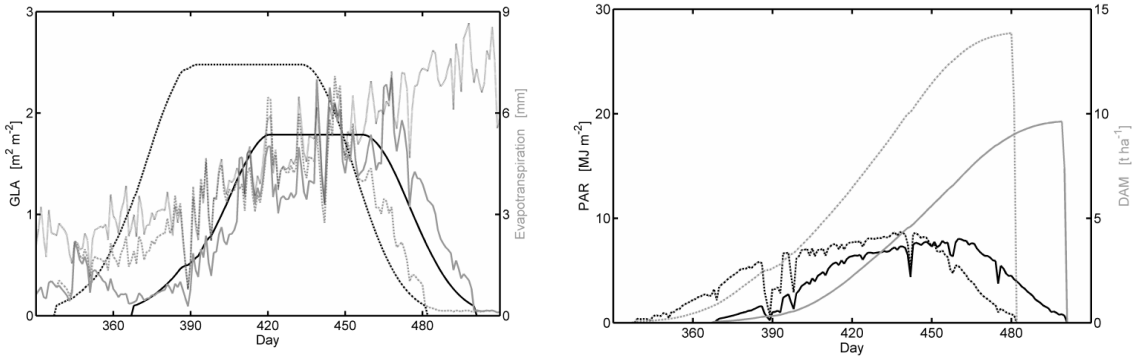

(**a**) (**b**)

Figure 9. Times courses of the main biophysical variables simulated for two fields representative of early (dotted lines) and late (full lines) sowing dates: (**a**) Green Leaf Area Index (black lines) and actual evapotranspiration (gray lines) simulated by the model, together with reference evapotranspiration (light gray dashed line); (**b**) photosynthetically-active radiation absorbed by the canopy (black lines) and dry aboveground mass (gray lines) simulated by the model. The days are numbered from 1 January 2007.

The previous statements and the trends illustrated in Figure 10 are somewhat contrasted by those of [42], which have analyzed the wheat response to sowing date using remote sensing estimates of yield during three agricultural seasons from 1999 to 2003. This study has shown that the relation between wheat yield and sowing date is variable from year to year: (i) for the 1999 to 2000 season, the yield was stable at a maximal value for a sowing date before 15 December; then, it decreased significantly; (ii) for the 2001 to 2002 season, the yield increased for the earliest sowing to an optimal period from 1 December to 1 January; and (iii) for the 2002 to 2003 season, the yield displayed a comparable level, whatever the sowing date. It should be also pointed out that the sowing date is not recognized as a primary factor of yield variation by [42], but climatic variability, soil properties and fertilization practices are [40–42]. The difference of point of view came from the study scale, which is the whole Yaqui Valley for these authors, whereas our study is limited to an 8 × 8 km^2, where the agro-environment (soil, climate, practices) is by far more homogeneous.

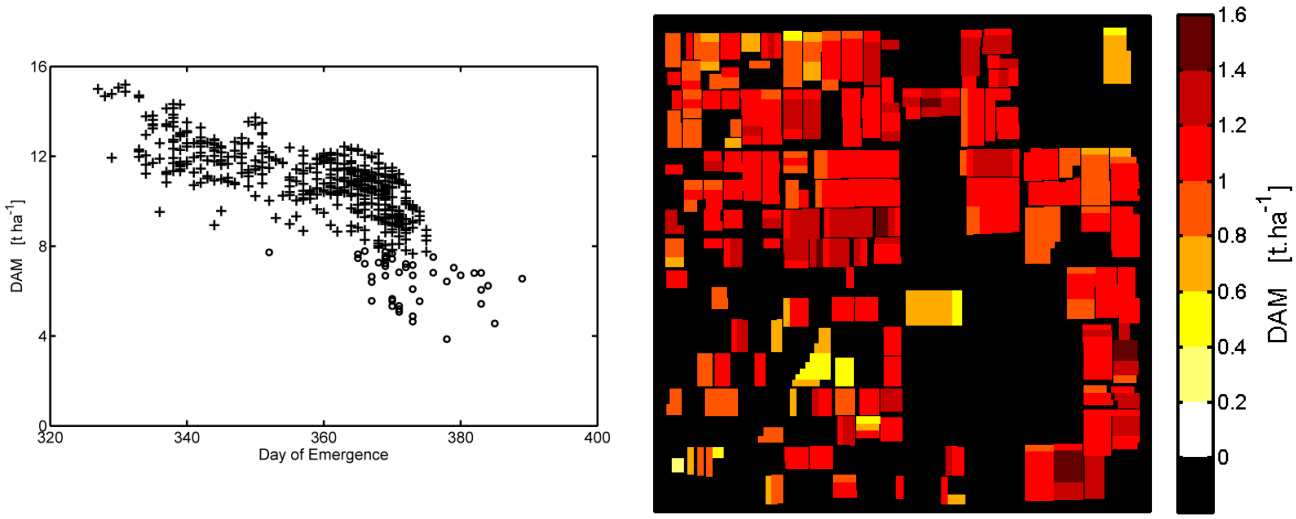

Figure 10. Dry aboveground mass as a function of the day of plant emergence (numbered from 1 January 2007). Circles indicate fields where the maximal Green Leaf Area Index did not exceed 1.5 (**left**). Spatial patterns of the dry aboveground mass (**right**).

In contrast to crop production, seasonal evapotranspiration did not vary as a function of the sowing date (Figure 11). The majority of the fields displayed a seasonal evapotranspiration in the range of 400 to 450 mm, whatever the day of plant emergence, when this variable was in the range of 330 to 375. Seasonal evapotranspiration was mainly related to the pattern of the Green Leaf Area Index, decreasing from 450 mm for the fields with the highest maximal GLA values to an interval of 300 to 400 mm on the fields with the lowest GLA values (see the circles in Figure 11). The latter occurred mainly on the fields for which sowing was delayed: it is always verified for the fields with a DoPE after 375 and, to a lesser extent, for some other fields with DoPE between 365 and 375. These fields experienced reduced plant development and, thus, reduced transpiration. This is always true for the field (day of plant emergence after 375). In any case, seasonal evapotranspiration appeared in the range of values found for wheat in the Yaqui Valley (e.g., [37,76]).

Finally, the crop production and the seasonal evapotranspiration were combined to compute the water use efficiency. The interval of variations of WUE (1.2 to 3.6 $kg \cdot m^{-3}$; Figure 12) appeared consistent with values derived from previous experiments on wheat crops, both in Mediterranean and in temperate climates [87,88]. Water use efficiency experienced a high variability, which is mainly explained by sowing practices: the determination coefficient between the day of plant emergence and the water use efficiency is 0.59. The values estimated on the fields sown the earliest were three-times higher than those estimated on the fields sown the latest. This is primarily explained by the variations of the crop production (see Figure 10), since seasonal evapotranspiration was not much impacted by sowing practices (see Figure 11). Not surprisingly, the fields where plant development was limited exhibited the lowest WUE value (circles in Figure 12).

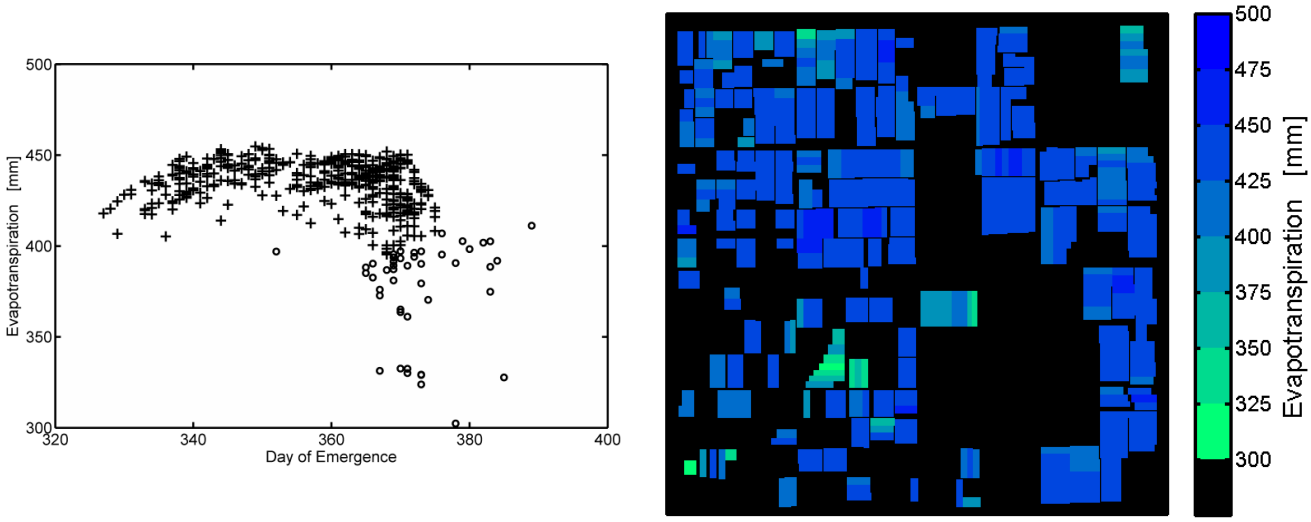

Figure 11. Seasonal evapotranspiration as a function of the day of plant emergence (numbered from 1 January 2007). Circles indicate fields where the maximal Green Leaf Area Index did not exceed 1.5 (**left**). Spatial patterns of the seasonal evapotranspiration (**right**).

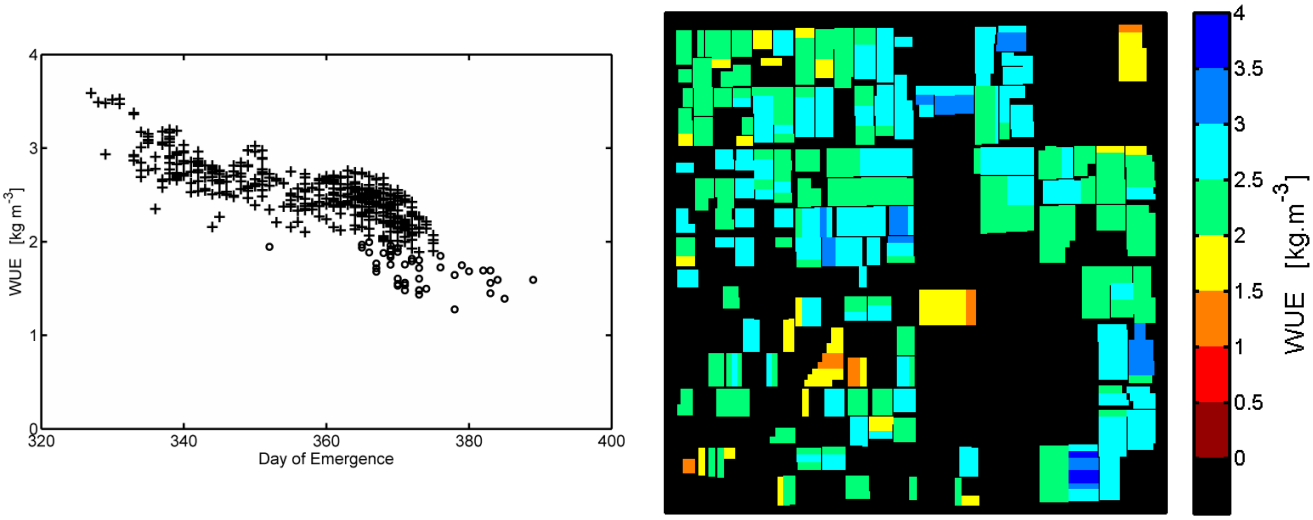

Figure 12. Water use efficiency as a function of the day of plant emergence (numbered from 1 January 2007). Circles indicate fields where the maximal green leaf area index did not exceed 1.5 (**left**). Spatial patterns of the water use efficiency (**right**).

5. Conclusions

In this study, a method was developed for providing spatial estimates of crop production, seasonal evapotranspiration and, then, water use efficiency. We used the SAFY-WB crop/water balance controlled by time series of a key biophysical variable, the Green Leaf Area index (GLA), derived from FORMOSAT-2 images acquired at both a high spatial resolution and a high temporal repetitiveness. This model was specifically designed to represent well-known processes involved in crop growth and water exchange within the soil-plant-atmosphere system, with the requirement that these processes can be represented using a minimal amount of data and formalisms, in order to make a regional study possible.

The method was evaluated for wheat crops cultivated within the large irrigated Yaqui Valley (the northwest of Mexico) during the 2007 to 2008 agricultural season. Using observations derived from FORMOSAT-2 images on up to 530 fields, it was first demonstrated that the SAFY-WB model is an excellent interpolator of GLA. There was also a good accuracy in the retrieval of the day of plant emergence, due to the availability of numerous GLA observations at the beginning of the agricultural season. In these conditions, the total dry aboveground biomass (DAM) was found to be strongly correlated with the grain yield ($R^2 > 0.8$) collected over 11 fields covering up to 120 ha by surveying harvesting machines, and the associated harvest index (about 0.43) was judged to be consistent with the values derived from many other previous experiment in the same area. We had a high degree of confidence in the simulations of crop production, though no specific calibration of the model was performed against biomass data. These performances were credited to the combined use of: (i) a model able to reproduce a large range of GLA seasonal patterns with a small number of parameters calibrated; and (ii) a remote sensing system providing a high density of observations across the entire growing season, both spatially (at field scale) and temporally (one image every five days).

Obtaining spatial estimates of evapotranspiration and other component of the water balance is not trivial over agricultural areas, since irrigation schedules, which have a large variability both in space and time, are generally not known. This case study within the Yaqui Valley may be rather simple in this respect, because we were out of drought periods and the water supply was guaranteed during the 2007 to 2008 experiment. Under the assumption (confirmed by the analysis of *in situ* data) that regular irrigations were operated to fulfill crop water requirements, evapotranspiration was estimated as an output of the SAFY-WB model. There was good agreement between simulated and measured soil moisture, and the comparison of simulations with evapotranspiration measured through the eddy correlation technique on two wheat fields during the experiment showed errors of about 20% at a daily step.

The previous statements demonstrate the interest in FORMOSAT-2 images in the description of the seasonality of vegetation, therefore strengthening the control of the crop/water balance model in time and space. The availability of numerous fine satellite observations also allowed a comprehensive analysis of the spatial variability of wheat crop production and water consumption. For that purpose, dry aboveground biomass (DAM) and seasonal evapotranspiration (ET) were simulated for up to 530 fields over an 8×8 km^2 irrigated area where the experiment took place. Each of these fields was a homogeneous spatial unit size of about 5 ha where wheat was cultivated.

Despite the low variability of soil and climatic conditions over the study area, we observed very large variations in crop production. The day of plant emergence was found to explain the major part of this variability, with a regular decreases of DAM from about 15 t·ha^{-1} for the fields sown the earliest to about 5 t·ha^{-1} for the fields sown the latest. In contrast, the seasonal ET did not experience such large variations: it ranged from 350 to 450 mm, with no evident link with sowing practices, except a decrease observed for the fields with both delayed sowing and reduced plant growth.

Finally, the water use efficiency (WUE) was estimated on a seasonal basis as the simple ratio of the dry aboveground mass divided by the seasonal evapotranspiration. As the amount of rainfall was low during the experiment, WUE is almost a direct measure of crop irrigation water productivity. Despite the fact that the study area was rather small and homogeneous (soil, climate), it was found that WUE varied from 1.5 to 3.5 kg·m^{-3}. The sowing date was the main factor responsible for the observed variation in WUE. This result reinforces the previous findings about the different agro-climatic

parameters that influence wheat yield in the Yaqui Valley, which have been derived from either local (pilot) experiments or at the scale of the whole irrigated area (through TM imagery). It also underlines the added value of satellite imaging systems at a high space and time resolution in the context of agro-meteorological studies.

Acknowledgments

The Yaqui 2007 to 2008 experiment was organized jointly by the IRD (Institut de Recherche pour le Développement), CESBIO (Centre d'Études Spatiales de la BIOsphère), ITSON (Instituto Tecnológico de SONora), UNISON (UNIversidad de SONora) and COLPOS (COLegio de POStgraduados) institutions with funding of the European Union (7th PCRD (Programme-Cadre de Recherche et de Développement technologique), PLEIADeS (Participatory multi-Level EO-assisted tools for Irrigation water management and Agricultural Decision-Support) program, http://www.pleiades.es/), the French INSU-PNTS (Institut National des Sciences de l'Univers—Programme National de Télédétection Spatiale) and CNES-TOSCA (Centre National d'Études Spatiales - Terre Océan Surface Continentale Atmosphère) programs and the Mexican CONACYT (COnsejo NAtional de Cienca Y Tecnologia) program. We are indebted to NSPO (National Space Organization), SPOT-Image and CNES for the delivery and the processing of FORMOSAT-2 images. We are grateful to the AERONET (AErosol RObotic NETwork) for their help in the acquisition of Cimel Sunphotometer data.

Author Contributions

Benoit Duchemin and Rémy Fieuzal are the principal authors of this manuscript having written and revised the manuscript and contributing at all phases of the investigation. The other co-authors contributed in the field logistics, the field design, the selection and the pre-processing of the experimental data or the satellite images.

Conflicts of Interest

The authors declare no conflict of interest.

References

1. FAO. Water Reports N°22. 2002. Available online: www.fao.org/docrep/004/Y3655E/y3655e00.htm (accessed on 13 December 2009).
2. World Bank. 2004. Water Resources Sector Strategy: Strategic Directions for World Bank Engagement. Available online: http://siteresources.worldbank.org/INTINFNETWORK/Resources/water.pdf (accessed on 13 December 2009).
3. UNESCO-WWAP. Climate Change and Water—An Overview from the World Water Development Report 3: Water in a Changing World. United Nations World Water Assessment Programme Special Report. 2009. Available online: unesdoc.unesco.org/images/0018/001863/186318e.pdf (accessed on 13 December 2009).

4. Qadir, M.; Boers, Th.M.; Schubert, S.; Ghafoor, A.; Murtaza, G. Agricultural water management in water-starved countries: Challenges and opportunities. *Agric. Water Manag.* **2003**, *62*, 165–185.
5. Qadir, M.; Sharma, B.R.; Bruggeman, A.; Choukr-Allah, R.; Karajeh, F. Non-conventional water resources and opportunities for water augmentation to achieve food security in water scarce countries. *Agric. Water Manag.* **2007**, *87*, 2–22.
6. IPCC. Climate Change and Water. International Panel on Climatic Chage—Technical Paper IV. 2008. Available online: www.ipcc.ch/pdf/technical-papers/climate-change-water-en.pdf (accessed on 13 December 2009).
7. Katerji, N.; Mastrorilli, M.; Rana, G. Water use efficiency of crops cultivated in the Mediterranean region: Review and analysis. *Eur. J. Agron.* **2008**, *28*, 493–507.
8. Bastiaanssen, W.G.M.; Allen, R.G.; Droogers, P.; D'Urso, G.; Steduto, P. Twenty-five years modeling irrigated and drained soils: State of the art. *Agric. Water Manag.* **2007**, *92*, 111–125.
9. Cassman, K.G.; Dobermann, A.; Walters, D.T.; Yang, H. Meeting cereal demand while protecting natural resources and improving environmental quality. *Annu. Rev. Environ. Resour.* **2003**, *28*, 315–358.
10. SIAP. Servicio de InformaciónAgroalimentaria y Pesquera, 2010. Available online: www.siap.sagarpa.gob.mx/ (accessed on 13 December 2009).
11. Naylor, R.L.; Falcon, W.P.; Puente-González, A. *Policy reforms and Mexican agriculture: Views from the Yaqui Valley*; CIMMYT Economics Program Paper, No. 01-01; CIMMYT: Mexico, D.F., Mexico, 2001.
12. Brito-Castillo, L.; Leyva-Contreras, A.; Shelutko, V.A.; LuchBelda, D. Pacific Decadal Oscillation and the filled capacity of dams on the rivers of the Gulf of California continental watershed. *Atmosféra* **2002**, *15*, 121–138.
13. Nicholas, R.E.; Battisti, D.S. Drought recurrence and seasonal rainfall prediction in the Rio Yaqui basin, Mexico. *J. Clim. Appl. Meteorol.* **2008**, *47*, 991–1005.
14. McCullough, E. Coping with Drought: An Analysis of Crisis Responses in the Yaqui Valley. Master's Thesis, Stanford University, Palo Alto, CA, USA, 2005. Available online: yaquivalley.stanford.edu/publications (accessed on 13 December 2009).
15. Schoups, G.; Addams, L.; Minjares, J.L.; Gorelick, S.M. Sustainable conjunctive water management in irrigated agriculture: Model formulation and application to the Yaqui Valley, Mexico. *Water Resourc. Res.* **2006**, *42*, W10417.
16. Dean, A.M. *Drought Enters Ninth Year in Birthplace of the Green Revolution. Encina Columns, Spring ed.*; Stanford Institute for International Studies, Stanford University: Palo Alto, CA, USA, 2004; p. 11. Available online: yaquivalley.stanford.edu/publications (accessed on 13 December 2009).
17. Briggs, L.J.; Shantz, H.L. *The Water Requirement of Plants. II: A Review of the Literature*; US Department of Agriculture, Bureau of Plant Industry: Washington, DC, USA, 1913; Volume 285
18. Sinclair, T.R.; Tanner, C.B.; Bennett, J.M. Water-use efficiency in CropProduction. *BioScience* **1984**, *34*, 36–40.
19. Van Duivenbooden, N.; Pala, M.; Studer, C.; Bielders, C.L.; Beukes, D.J. Cropping systems and crop complementarity in dryland agriculture to increase soil water use efficiency: A review. *Wagening. J. Life Sci./Neth. J. Agric. Sci.* **2000**, *48*, 213–236.

20. Green, T.R.; Yu, Q.; Ma, L. Crop water use efficiency at multiple scales. *Agric. Water Manag.* **2010**, *97*, 1099–1101.
21. Kijne, J.W., Barker, R., Molden, D.J., Eds. *Water Productivity in Agriculture: Limits and Opportunities for Improvement*; CABI: North Wyke, Devon, UK, 2003; p. 332.
22. Ayars, J.E.; Phene, C.J.; Hutmacher, R.B.; Davis, K.R.; Schoneman, R.A.; Vail, S.S.; Mead, R.M. Subsurface drip irrigation of row crops: A review of 15 years of research at the Water Management Research Laboratory. *Agric. Water Manag.* **1999**, *42*, 1–27.
23. Geerts, S.; Raes, D. Deficit irrigation as an on-farm strategy to maximize crop water productivity in dry areas. *Agric. Water Manag.* **2009**, *96*, 1275–1284.
24. Garcia y Garcia A.; Persson, T.; Guerra, L.C.; Hoogenboom, G. Response of soybean genotypes to different irrigation regimes in a humid region of the southeastern USA. *Agric. Water Manag.* **2010**, *97*, 981–987.
25. Chen S.; Zhang, X.; Sun, H.; Ren, T.; Wang, Y. Effects of winter wheat row spacing on evapotranpsiration, grain yield and water use efficiency. *Agric. Water Manag.* **2010**, *97*, 1126–1132.
26. Blum, A. Effective use of water (EUW) and not water-use efficiency (WUE) is the target of crop yield improvement under drought stress. *Field Crops Res.* **2009**, *112*, 119–123.
27. Zoebl, D. Is water productivity a useful concept in agricultural water management? *Agric. Water Manag.* **2006**, *84*, 265–273.
28. Chern, J.S.; Ling, J.; Weng, S.L. Taiwan's second remote sensing satellite. *Acta Astronaut.* **2008**, *63*, 1305–1311.
29. Hagolle, O.; Dedieu, G.; Mougenot, B.; Debaecker, V.; Duchemin, B.; Meygret, A. Correction of aerosol effects on multi-temporal images acquired with constant viewing angles: Application to Formosat-2 images. *Remote Sens. Environ.* **2008**, *112*, 1689–1701.
30. Courault, D.; Bsaibes, A.; Kpemlie, E.; Hadria, R.; Hagolle, O.; Marloie, O.; Hanocq, J.F.; Olioso, A.; Bertrand, N.; Desfonds, V.; *et al*. Assessing the potentialities of FORMOSAT-2 Data for water and crop monitoring at small regional scale in South-Eastern France. *Sensors* **2008**, *8*, 3460–3481.
31. Duchemin, B.; Hagolle, O.; Mougenot, B.; Simonneaux, V.; Benhadj, I.; Hadria, R.; Ezzahar, J.; Hoedges, J.; Khabba, S.; Kharrou, M.H.; *et al*. Agrometerological study of semi-arid areas: An experiment for analysing the potential of FORMOSAT-2 time series of images in the Marrakech plain. *Int. J. Remote Sens.* **2008**, *29*, 5291–5299.
32. Bsaibes, A.; Courault, D.; Baret, F.; Weiss, M.; Olioso, A.; Jacob, F.; Hagolle, O.; Marloie, O.; Bertrand, N.; Desfond, V.; *et al*. Albedo and LAI estimates from FORMOSAT-2 data for crop monitoring. *Remote Sens. Environ.* **2009**, *113*, 716–729.
33. Hadria, R.; Duchemin, B.; Baup, F.; le Toan, T.; Bouvet, A.; Dedieu, G.; le Page, M. Combined use of optical and radar satellite data for the detection of tillage and irrigation operations: Case study in Central Morocco. *Agric. Water Manag.* **2009**, *96*, 1120–1127.
34. Hadria, R.; Duchemin, B.; Jarlan, L.; Dedieu, G.; Baup, F.; Khabba, S.; Olioso, A.; le Toan, T. Potentiality of optical and radar satellite data at high spatio-temporal resolutions for the monitoring of irrigated wheat crops in Morocco. *Int. J. Appl. Earth Obs. Geoinf.* **2010**, *12S*, S32–S37.

35. Limon-Ortega, A.; Sayre, K.D.; Drijber, R.A.; Francis, C.A. Soil attributes in a furrow-irrigated bed planting system in northwest Mexico. *Soil Tillage Res.* **2002**, *63*, 123–132.
36. Luers, A.L.; Lobell, D.B.; Sklar, L.S.; Addams, C.L.; Matson, P.A. A method for quantifiying vulnerability, applied to the agricultural system of the Yaqui Valley, Mexico. *Glob. Environ. Chang.* **2003**, *13*, 255–267.
37. Rodriguez, J.C.; Duchemin, B.; Hadria, R.; Watts, C.; Garatuza-Payan, J.; Chehbouni, A.; Khabba, S.; Boulet, G.; Palacios, R.; Lahrouni, A.; *et al*. Wheat yield estimation using remote sensing and the STICS model in the semiarid valley of Yaqui, Mexico. *Agronomie* **2004**, *24*, 295–304.
38. Schoups, G.; Addams, L.; Gorelick, S. Multi-objective calibration of a surface water-groundwater flow model in an irrigated agricultural region: Yaqui Valley, Sonora, Mexico. *Hydrol. Earth Syst. Sci.* **2005**, *9*, 549–568.
39. Lobell, D.B.; Asner, G.P.; Ortiz-Monasterio, J.I.; Benning, T.L. Remote sensing of regional crop production in the Yaqui Valley, Mexico: Estimates and uncertainties. *Agric. Ecosyst. Environ.* **2003**, *94*, 205–220.
40. Lobell, D.B.; Ortiz-Monasterio, J.I.; Asner, G.P.; Naylor, R.L.; Falcon, W.P. Combining field surveys, remote sensing, and regression trees to understand yield variations in an irrigated wheat landscape. *Agron. J.* **2005**, *97*, 241–249.
41. Lobell, D.B.; Ortiz-Monasterio, J.I. Regional importance of crop yield constraints: Linking simulation models and geostatistics to interpret spatial patterns. *Ecol. Model.* **2006**, *196*, 173–182.
42. Ortiz-Monasterio, J.I.; Lobell, D.B. Remote sensing assessment of regional yield losses due to sub-optimal planting dates and fallow period weed management. *Field Crops Res.* **2007**, 101, 80–87.
43. Chehbouni, A.; Hoedjes, J.C.B.; Rodriquez, J.C.; Watts, C.J.; Garatuza-Payan, J.; Jacob, F.; Kerr, Y.H. Using remotely sensed data to estimate area-averaged daily surface fluxes over a semi-arid mixed agricultural land. *Agric. For. Meteorol.* **2008**, *148*, 330–342.
44. Mendez-Barroso, L.A.; Garatuza-Payan, J.; Vivoni, E.R. Quantifying water stress on wheat using remote sensing in the Yaqui Valley, Sonora, Mexico. *Agric. Water Manag.* **2008**, *95*, 725–736.
45. Merlin, O.; Duchemin, B.; Hagolle, O.; Jacob, F.; Coudert, B.; Chehbouni, A.; Dedieu, G.; Garatuza-Payan, J.; Kerr, Y. Disaggregation of MODIS surface temperature over an agricultural area using a time series of Formosat-2 images. *Remote Sens. Environ.* **2010**, doi:10.1016/j.rse.2010.05.025.
46. Lagouarde, J.P.; Mac Aneney, K.J. Daily sensible heat flux estimation from a single measurement of surface temerature and maximum air temperature. *Bound. Layer Meteorol.* **1992**, *59*, 341–362.
47. Gavilan, P.; Berengena, J.; Allen, R.G. Measuring *versus* estimating net radiation and soil heat flux: Impact on Penman-Monteith reference ET estimates in semiarid regions. *Agric. Water Manag.* **2007**, *89*, 275–286.
48. Chirouze, J.; Boulet, G.; Jarlan, L.; Fieuzal, R.; Rodriguez, J.C.; Ezzahar, J.; Er-Raki, S.; Bigeard, G.; Merlin, O.; Garatuza-Payan, J.; *et al*. Intercomparison of four remote-sensing-based energy balance methods to retrieve surface evapotranspiration and water stress of irrigated fields in semi-arid climate. *Hydrol. Earth Syst. Sci.* **2014**, *18*, 1165–1188.

49. Demarez, V.; Duthoit, S.; Baret, F.; Weiss, M.; Dedieu, G. Estimation of leaf area and clumping indexes of crops with hemispherical photographs. *Agric. For. Meteorol.* **2008**, *148*, 644–655.
50. Welles, J.M.; Norman, J.M. Instrument for indirect measurement of canopy architecture. *Agron. J.* **1991**, *83*, 818–825.
51. Wagner, B.; Tarnawski, V.R.; Hennings, V.; Müller, U.; Wessolek, G.; Plagge, R. Evaluation of pedo-transfer functions for unsaturated soil hydraulic conductivity using an independent data set. *Geoderma* **2001**, *102*, 275–297.
52. Boulet, G.; Mougenot, B.; ben Abdelouahab, T. An evaporation test based on Thermal Infra Red Remote-Sensing to select appropriate soil hydraulic properties. *J. Hydrol.* **2009**, *376*, 589–598.
53. Rawls, W.J.; Brakensiek, D.L.; Saxton, K.E. Estimation of soil water properties. *Trans. ASAE* **1982**, *25*, 1316–1320, 1328.
54. National Space Organization. Available online: http://www.nspo.org.tw (accessed on 13 December 2009).
55. Airbus Defence and Space. Available online: http://www.spotimage.com (accessed on 13 December 2009).
56. Rahman, H.; Dedieu, G. SMAC: A simplified method for the atmospheric correction of satellite measurements in the solar spectrum. *Int. J. Remote Sens.* **1994**, *15*, 123–143.
57. Rouse, J.W.; Haas, R.H.; Schell, J.A.; Deering, D.W.; Harlan, J.C. *Monitoring the Vernal Advancement and Retrogradation of Natural Vegetation*; Type III, Final Report; NASA United States: Greenbelt, MD, USA, 1974.
58. Duchemin, B.; Maisongrande, P.; Boulet, G.; Benhadj, I. A simple algorithm for yield estimates: Evaluation for semi-arid irrigated winter wheat monitored with ground-based remotely-sensed data. *Environ. Model. Softw.* **2008**, *23*, 876–892.
59. Allen, R.G.; Pereira, L.S.; Raes, D.; Smith, M. *Crop Evapotranspiration: Guidelines for Computing Crop Water Requirements*; FAO Irrigation and Drainage Paper 56; FAO Natural Resources Management and Environment Department: Rome, Italy, 1998; p. 300.
60. Allen, R.G. Using the FAO-56 dual crop coefficient method over an irrigated region as part of an evapotranspiration intercomparison study. *J. Hydrol.* **2000**, *229*, 27–41.
61. Monteith, J.L. Climate and the efficiency of crop production in Britain. *Philos. Trans. R. Soc. Lond. Ser. B* **1977**, *281*, 277–294.
62. Monsi, M.; Saeki, T. Über den Lichtfactor in den Pflanzengesellschaften und Seine Bedeutungfürdie Stoffproduction. *Jpn. J. Bot.* **1953**, *14*, 22–52.
63. Maas, S.J. Parameterized model of gramineous crop growth: I. Leaf area and dry mass simulation. *Agron. J.* **1993**, *85*, 348–353.
64. Porter, J.R.; Gawith, M. Temperatures and the growth and development of wheat: A review. *Eur. J. Agron.* **1999**, *10*, 23–36.
65. Brisson, N.; Gary, C.; Justes, E.; Roche, R.; Mary, B.; Ripoche, D.; Zimmer, D.; Sierra, J.; Bertuzzi, P.; Burger, P.; *et al*. An overview of the crop model STICS. *Eur. J. Agron.* **2003**, *18*, 309–322.

66. Claverie, M.; Demarez, V.; Duchemin, B.; Maire, F.; Hagolle, O.; Keravec, P.; Marciel, B.; Ceschia, E.; Dejoux, J.F.; Dedieu, G.; *et al*. Spatialisation of crop Leaf Area Index and Biomass by combining a simple crop model and high spatial and temporal resolutions remote sensing data. In Proceedings of 2009 IEEE International Geoscience And Remote Sensing Symposium, Cape Town, South Africa, 13–17 July 2009.
67. Fieuzal, R.; Duchemin, B.; Jarlan, L.; Baup, F.; Augustin Rivera, M.A.; Perez-Ruiz, E.R.; Garatuza-Payan, J.; Boulet, G.; Zribi, M.; Hadria, R.; *et al*. Potential of ENVISAT/ASAR time series for the monitoring of surface vegetation and soil changes in irrigated arid croplands: Case study in the Yaqui Valley (Sonora, Mexico). In Proceedings of 2009 ESA International Conference on Earth Observation and Water Cycle Science, Frascati, Italy, 18–20 November 2009.
68. Asrar, G.; Fuchs,M.; Kanemasu, E.T.; Hatfield, J.L. Estimating absorbed photosynthetic radiation and leaf area index from spectral reflectance in wheat. *Agron. J.* **1984**, *76*, 300–306.
69. Baret, F.; Guyot, G. Potentials and limits of vegetation indices for LAI and APAR assessment. *Remote Sens. Environ.* **1991**, *35*, 161–173.
70. Duchemin, B.; Hadria, R.; Er-Raki, S.; Boulet, G.; Maisongrande, P.; Chehbouni, A.; Escadafal, R.; Ezzahar, J.; Hoedjes, K.; Kharrou, M.H.; *et al*. Monitoring wheat phenology and irrigation in Center of Morocco: On the use of relationship between evapotranspiration, crops coefficients, leaf area index and remotely-sensed vegetation indices. *Agric. Water Manag.* **2006**, *79*, 1–27.
71. Devonec, E.; Barros, A.P. Exploring the transferability of a land-surface hydrology model. *J. Hydrol.* **2002**, *265*, 258–282.
72. Smith, M.; Allen, R.G.; Monteith, J.L.; Pereira, L.S.; Perrier, A.; Pruitt, W.O. *Report on the Expert Consultation on Procedures for Revision of FAO Guidelines for Prediction of Crop Water Requirements*; Land and Water Development Division, United Nations Food and Agriculture Service: Rome, Italy, 1992.
73. Allen, R.G.; Smith, M.; Perrier, A.; Pereira, L.S. An update for the definition of reference evapotranspiration. *ICID Bull.* **1994**, *43*, 1–82.
74. Deardorff, J.W. Efficient prediction of ground surface temperature and moisture, with inclusion of a layer of vegetation. *J. Geophys. Res.* **1978**, *83C*, 1889–1903.
75. Reynolds M.; Dreccer, F.; Trethowan, R. Drought-adaptive traits derived from wheat wild relatives and landraces. *J. Exp. Bot.* **2007**, *58*, 177–186.
76. Zwart, S.J.; Bastiaanssen, W.G.M. SEBAL for detecting spatial variation of water productivity and scope for improvement in eight irrigated wheat systems. *Agric. Water Manag.* **2007**, *89*, 287–296.
77. Weiss, M.; Baret, F.; Smith, G.J.; Jonckheere, I.; Coppin, P. Review of methods for *in situ* leaf area index (LAI) determination: Part II. Estimation of LAI, errors and sampling. *Agric. For. Meteorol.* **2004**, *121*, 37–53.
78. Moulin, S.; Bondeau, A.; Delécolle, R. Combining agricultural crop models and satellite observations from field to regional scales. *Int. J. Remote Sens.* **1998**, *19*, 1021–1036.
79. Guérif, M.; Duke, C. Crop model spatial adjustment using remote sensing: Effect of soils and crops variability at regional scale. *Agric. Ecosyt. Environ.* **2000**, *81*, 57–69.
80. Del Blanco, I.A.; Rajaram, S.; Kronstad, W.E. Agronomic potential of synthetic hexaploid wheat-derived populations. *Crop Sci.* **2001**, *41*, 670–676.

81. Limon-Ortega, A.; Sayre, K.D.; Francis, C.A. Wheat and maize yields in response to straw management and nitrogen under a bed planting system. *Agron. J.* **2000**, *92*, 295–302.
82. Manske, G.G.B.; Ortiz-Monasterio, J.I.; van Ginkel, M.; Gonzalez, R.M.; Fischer, R.A. Rajaram, S.; Vlek, P.L.G. Importance of P uptake efficiency *versus* P utilization for wheat yield in acid and calcareous soils in Mexico. *Eur. J. Agron.* **2001**, *14*, 261–274.
83. Del Blanco, I.A.; Rajaram, S.; Kronstad, W.E.; Reynolds, M.P. Physiological performances of synthetic hexaploid wheat-derived populations. *Crop Sci.* **2000**, *40*, 1257–1263.
84. Hoedjes, J.C.B.; Chehbouni, A.; Ezzahar, J.; Escadafal, R.; de Bruin, H.A.R. Comparison of large aperture scintillometer and eddy covariance measurements: Can thermal infrared data be used to capture footprint-induced differences? *J. Hydrometeorol.* **2007**, *8*, 194–206.
85. Boulet, G.; Chehbouni, A.; Gentine, P.; Duchemin, B.; Ezzahar, J.; Hadria, R. Monitoring water stress using time series of observed to unstressed surface temperature difference. *Agric. For. Meteorol.* **2007**, *146*, 159–172.
86. Limon-Ortega, A.; Govaerts, B.; Sayre, K.D. Straw management, crop rotation, and nitrogen source effect on wheat grain yield and nitrogen use efficiency. *Eur. J. Agron.* **2008**, *29*, 21–28.
87. Oweis, T.; Zhang, H.; Pala, M. Water use efficiency of rainfed and irrigated bread wheat in a Mediterranean environment. *Agron. J.* **2000**, *92*, 231–238.
88. Tallec, T.; Béziat, P.; Jarosz, N.; Rivalland, V.; Ceschia, E. Crops' water use efficiencies in temperate climate: Comparison of stand, ecosystem and agronomical approaches. *Agric. For. Meteorol.* **2013**, *168*, 69–81.